Supporting Information for

" Pillar Iodination in Functional Boron Cage Hybrid Supramolecular Frameworks for High Performance Separation of Light Hydrocarbons "

Dr. Yuanbin Zhang, [ab] Lifeng Yang, [ab] Dr. Lingyao Wang,[c]

Dr. Xili Cui,[ab] Dr. Huabin Xing*[ab]

[a] Dr. Y. Zhang, L. Yang, Dr. X. Cui, Dr. H. Xing*

Key laboratory of Biomass Chemical Engineering of Ministry of Education,

College of Chemical and Biological Engineering

Zhejiang University, Hangzhou 310027, China

E-mail: xinghb@zju.edu.cn

[b] Dr. Y. Zhang, L. Yang, Dr. X. Cui, Dr. H. Xing*

Institute of Zhejiang University - Quzhou, 78 Jiuhua Boulevard North, Quzhou 324000, China.

[c] Dr. L. Wang

Department of Chemistry, Zhejiang University, Hangzhou 310027, China.

I General Information and Procedures

Unless otherwise noted, all the reactions were performed under air without N_2 or Ar protection. All reagents were used as received without purification unless stated otherwise.

Chemicals: The basic starting material $[Na]_2[B_{12}H_{11}I]$ was readily prepared by reported methods.[1] 1,2-bis(4-pyridyl)acetylene and 4,4'-azobispyridine were purchased from Chemsoon without further purification. $Cu[NO_3]_2 \cdot 3H_2O$ and All other reagents were purchased from Adamas-beta and used without further purification.

Preparation of BSF-2

A mixture of $[Na]_2[B_{12}H_{11}I]$ (314 mg, 1 mmol, 1 equiv) and $Cu[NO_3]_2 \cdot 3H_2O$ (242 mg, 1 mmol, 1 equiv) was dissolved in 10 mL of water in a 100 mL round bottom flask. Then a MeOH (15 mL) solution of 1, 2-bis(4-pyridyl)acetylene (360 mg, 2 mmol, 2 equiv) was slowly added to the above aqueous solution. A violet solid precipitated immidiately, and the suspension was stirred at 25 °C for 24 h. The solid was collected by filtration and re-soaked in MeOH for solvent exchange. (Replacement of H_2O in the pores by MeOH benefits the activation of BSF-2 under vacuum for adsorption experiments)

Characterization:

IR spectra were recorded on a Nicolet iS10 FT-IR spectrometer as KBr pellets.

Single-crystal X-ray diffraction studies were conducted at 173 K on a BrukerAXS D8 VENTURE diffractometer equipped with a PHOTON-100/CMOS detector (CuKα, λ = 1.5418 Å; Mo-Kα λ=0.71073 Å). Indexing was performed using APEX2. Data integration and reduction were completed using SaintPlus 6.01. Absorption correction was performed by the multi-scan method implemented in SADABS. The space group was determined using XPREP implemented in APEX2.1 The structure was solved with SHELXS-97 (direct methods) and refined on F2 (nonlinear least-squares method) with SHELXL-97 contained in APEX2, WinGX v1.70.01, and OLEX2 v1.1.5 program packages. All non-hydrogen atoms were refined anisotropically. The contribution of disordered solvent molecules was treated as diffuse using the Squeeze routine implemented in Platon.

Powder X-ray diffraction (PXRD) data were collected on a SHIMADZU XRD-6000

diffractometer (Cu Kαλ = 1.540598 Å) with an operating power of 40 KV, 30mA and a scan speed of 4.0°/min. The range of 2θ was from 5° to 80°.

Thermal gravimetric analysis was performed on a TGA Q500 V20.13 Build 39 instrument. Experiments were carried out using a platinum pan under nitrogen atmosphere which conducted by a flow rate of 60 mL/min nitrogen gas. First, the sample was heated at 80 °C for 1 h to remove the water residue and equilibrated for 5 minutes, then cooled down to 50 °C. The data were collected at the temperature range of 50 °C to 800 °C with a ramp of 10 °C /min.

EPR spectra were collected on a computer controlled X-band (9.5GHz) EPR spectrometer (Bruker A300).

The gas adsorption measurements were performed on a Micromeritics ASAP 2460 instrument. Before gas adsorption measurements, the sample was evacuated at 80 ºC for 1 day until the pressure dropped below 7 μmHg. The sorption isotherms were collected at 273–313 K on activated samples.

The breakthrough experiments were carried out in a dynamic gas breakthrough equipment.[2-3] All experiments were conducted using a stainless steel column (0.46 cm inner diameter × 5 cm length. The weight of BSF-2 packed in the column was 0.2808 g. The column packed with sample was first purged with a He flow (5 mL min^{-1}) for 12 h at room temperature. The mixed gas of $C_3H_8/C_2H_6/CH_4$ = 5/10/85 (v/v/v) was then introduced at 4 mL min^{-1}. Outlet gas from the column was monitored using gas chromatography (GC-490) with the thermal conductivity detector TCD. After the breakthrough experiment, the sample was regenerated with a He flow of 5 mL min^{-1} under 40 °C for 8 h for repeated breakthrough experiments and other breakthrough experiments with gas mixture of C_2H_2/CO_2/He (10/5/85,v/v/v), CO_2/CH_4 (15/85, v/v) and C_2H_2/CH_4 (50/50, v/v). The sample in the column after regeneration was usually sealed and stored in the glovebox filled with N_2 for further use.

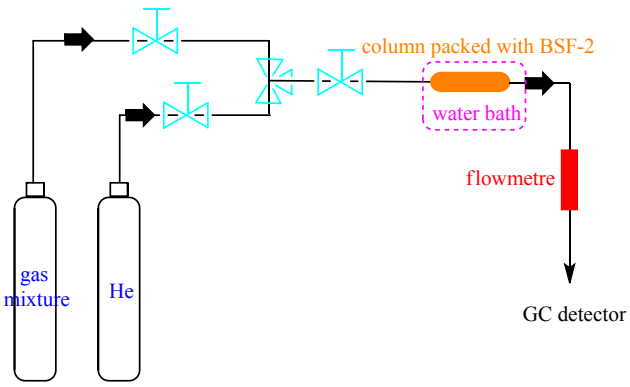

The shape of isotherm curves indicates that the adsorption of hydrocarbons on BSF-2 is not a simple monolayer adsorption (Langmuir type) because their capacities do not reach saturation at high pressure. In addition, the surface of BSF-1 is energetically uniform. In these cases, the dual-site Langmuir-Freundlich isotherm model is a reasonable selection for the correction of adsorption data. As evidence, the Q_{st} value calculated based on the fitting of dual-site Langmuir-Freundlich model is consistent with the calculated sorbate-sorbent interaction energy.

Fitting of pure component isotherms: the adsorption isotherms in BSF-2 were fitted using a dual-site Langmuir-Freundlich model.

$$q = q_{A,\ sat}\frac{b_A p^{v_A}}{1 + b_A p^{v_A}} + q_{B,\ sat}\frac{b_B p^{v_B}}{1 + b_B p^{v_B}} \qquad (1)$$

Here, P is the pressure of the bulk gas at equilibrium with the adsorbed phase (kPa), q is the adsorbed amount per mass of adsorbent (mol kg^{-1}), $q_{A,sat}$ an $q_{B,sat}$ are the saturation capacities of site A and B (mol kg^{-1}), b_A and b_B are the affinity coefficients of site A and B (kPa^{-1}), and v_A and v_B represent the deviations from an ideal homogeneous surface.

The binding energy is reflected in the isosteric heat of adsorption, Qst, defined as:

$$Q_{st} = RT^2\left(\frac{\partial \ln p}{\partial T}\right)_q \qquad (2)$$

The calculations are based on the use of the Clausius-Clapeyron equation.

The IAST adsorption selectivity for two gases is defined as:

$$S_{ads} = \frac{q_1/q_2}{p_1/p_2} \quad (3)$$

q_1, and q_2 are the molar loadings in the adsorbed phase in equilibrium with the bulk gas phase with partial pressures p_1, and p_2

Density-functional theory calculations: The static binding energy was calculated using the combination of first-principle density functional theory (DFT) and plane-wave ultrasoft pseudopotentil implemented in the Materials Studio, CASTEP code. Calculations were performed under the generalized gradient approximation (GGA) with Perdew-Burke-Ernzerhof (PBE) exchange correlation. A cutoff energy of 544 eV and a 2×2×3 k-point mesh were found to be enough for the total energy to converge within 1×10^{-5} ev atom^{-1}. The initial structure of BSF-2 with adsorbed gas was obtained from the results of GCMC simulation. The static binding energy (at T=0 K) was then calculated: EB = E (BSF-2) + E (gas) - E (BSF-2 + gas).

II X-ray Crystallography Data

Table S1. Crystal data and structure refinement for BSF-2

Empirical formula	C24 H27 B12 Cu I N4
Formula weight	691.65
Temperature	173(2) K
Wavelength	0.71073 Å
Crystal system	Monoclinic
Space group	C2/c
Unit cell dimensions	a = 28.398(2) Å α= 90° b = 17.7840(12) Å β= 133.929(2)° c = 20.2046(15) Å γ = 90°
Volume	7348.9(10) $Å^3$
Z	8
Density (calculated)	1.250 g/cm^3
Absorption coefficient	1.454 mm^{-1}
F(000)	2728
Crystal size	0.220 x 0.190 x 0.160 mm^3
Theta range for data collection	2.489 to 25.009°
Index ranges	-31<=h<=33, -20<=k<=21, -22<=l<=24
Reflections collected	23859
Independent reflections	6440 [R(int) = 0.0692]
Completeness to theta = 25.009°	99.5 %
Refinement method	Full-matrix least-squares on F^2
Data / restraints / parameters	6440 / 12 / 388
Goodness-of-fit on F^2	1.150
Final R indices [I>2sigma(I)]	R1 = 0.1525, wR2 = 0.3725
R indices (all data)	R1 = 0.1579, wR2 = 0.3750
Extinction coefficient	n/a
Largest diff. peak and hole	1.754 and -1.389 e. $Å^{-3}$

Table S2 Atomic coordinates (x10^4) and equivalent isotropic displacement parameters ($Å^2$ x 10^3) for BSF-2. U(eq) is defined as one third of the trace of the orthogonalized U^{ij} tensor

	x	y	z	U(eq)
Cu(1)	6992(1)	5005(1)	5725(1)	17(1)
I(1)	1388(1)	6019(2)	910(2)	54(1)
I(1')	1862(1)	6762(1)	66(1)	31(1)
N(1)	2629(5)	861(6)	1258(8)	24(3)
N(4)	11333(5)	9145(6)	10136(7)	23(2)
N(3)	7736(5)	5723(6)	6578(8)	20(2)
N(2)	6244(5)	4279(6)	4958(8)	21(2)
C(23)	11329(7)	8675(7)	10611(9)	24(3)
C(18)	8218(6)	5569(8)	7470(9)	25(3)
C(5)	3128(7)	808(8)	1312(11)	30(3)
C(4)	3623(7)	1344(9)	1773(11)	35(4)
C(24)	10838(7)	9128(8)	9196(9)	28(3)
C(14)	7772(7)	6375(8)	6288(10)	31(3)
C(10)	6170(6)	3793(7)	4364(9)	22(3)
C(9)	5625(7)	3338(9)	3791(10)	31(3)
C(1)	2618(8)	1459(8)	1656(12)	36(4)
C(13)	5237(7)	3841(9)	4408(10)	35(4)
C(17)	8756(7)	6038(10)	8098(11)	38(4)
C(22)	10846(7)	8128(8)	10232(11)	30(3)
C(12)	5765(7)	4314(8)	4943(10)	28(3)
C(6)	4124(7)	2464(9)	2732(11)	36(4)
C(25)	10333(7)	8610(8)	8742(10)	33(4)
C(8)	5139(7)	3363(7)	3782(11)	29(3)
C(3)	3595(8)	1954(9)	2185(11)	35(4)
C(19)	9340(8)	7192(9)	8357(13)	46(5)
C(16)	8796(8)	6687(8)	7787(12)	37(4)
C(21)	10319(7)	8109(8)	9276(11)	33(4)
B(1)	3727(9)	5425(11)	2803(12)	34(4)
C(2)	3060(8)	2022(9)	2064(12)	41(4)
B(2)	3422(9)	5901(10)	1804(12)	32(4)
C(15)	8297(8)	6876(9)	6846(12)	41(4)
B(3)	2950(8)	5206(8)	878(12)	27(3)
B(4)	3674(8)	4921(12)	2004(12)	36(4)

C(20)	9778(8)	7609(10)	8778(12)	43(4)
B(5)	2947(10)	4357(9)	1301(15)	35(4)
B(6)	3440(9)	4493(10)	2529(13)	33(4)
B(7)	2333(10)	5455(12)	1524(15)	45(5)
B(8)	3062(9)	6039(10)	2218(12)	38(5)
B(9)	2578(9)	4510(12)	1739(16)	43(5)
B(10)	2261(8)	4952(13)	707(14)	44(5)
C(7)	4585(9)	2901(10)	3192(12)	47(5)
B(11)	3061(8)	5157(11)	2652(12)	36(4)
B(12)	2589(10)	5902(12)	1029(14)	48(6)

Table S3 Selected bond lengths [Å] and angles [°] for BSF-2

Cu(1)-N(3)	2.003(11)
Cu(1)-N(2)	2.003(10)
Cu(1)-N(4)#1	2.030(11)
Cu(1)-N(1)#2	2.024(10)
I(1)-B(7)	2.26(2)
I(1')-B(12)	2.19(2)
N(1)-C(1)	1.350(19)
N(1)-C(5)	1.346(19)
N(4)-C(23)	1.277(18)
N(4)-C(24)	1.371(17)
N(3)-C(14)	1.336(18)
N(3)-C(18)	1.331(17)
N(2)-C(12)	1.340(18)
N(2)-C(10)	1.371(17)
C(23)-C(22)	1.400(18)
C(23)-H(23)	0.9500
C(18)-C(17)	1.40(2)
C(18)-H(18)	0.9500
C(5)-C(4)	1.390(19)
C(5)-H(5)	0.9500
C(4)-C(3)	1.40(2)
C(4)-H(4)	0.9500
C(24)-C(25)	1.385(19)
C(24)-H(24)	0.9500
C(14)-C(15)	1.40(2)
C(14)-H(14)	0.9500
C(10)-C(9)	1.380(18)
C(10)-H(10)	0.9500
C(9)-C(8)	1.37(2)
C(9)-H(9)	0.9500
C(1)-C(2)	1.35(2)
C(1)-H(1)	0.9500
C(13)-C(8)	1.38(2)
C(13)-C(12)	1.370(19)
C(13)-H(13)	0.9500

C(17)-C(16) 1.36(2)
C(17)-H(17) 0.9500
C(22)-C(21) 1.40(2)
C(22)-H(22) 0.9500
C(12)-H(12) 0.9500
C(6)-C(7) 1.22(2)
C(6)-C(3) 1.41(2)
C(25)-C(21) 1.42(2)
C(25)-H(25) 0.9500
C(8)-C(7) 1.40(2)
C(3)-C(2) 1.37(2)
C(19)-C(20) 1.16(2)
C(19)-C(16) 1.43(2)
C(16)-C(15) 1.41(2)
C(21)-C(20) 1.42(2)
B(1)-B(6) 1.76(3)
B(1)-B(4) 1.76(3)
B(1)-B(8) 1.75(2)
B(1)-B(11) 1.76(2)
B(1)-B(2) 1.76(2)
B(1)-H(1A) 1.1200
C(2)-H(2) 0.9500
B(2)-B(12) 1.70(3)
B(2)-B(8) 1.73(3)
B(2)-B(3) 1.83(2)
B(2)-B(4) 1.82(3)
B(2)-H(2A) 1.1200
C(15)-H(15) 0.9500
B(3)-B(5) 1.74(2)
B(3)-B(10) 1.79(3)
B(3)-B(12) 1.76(2)
B(3)-B(4) 1.78(2)
B(3)-H(3) 1.1200
B(4)-B(6) 1.77(3)
B(4)-B(5) 1.79(3)
B(4)-H(4A) 1.1200

B(5)-B(10) 1.76(3)
B(5)-B(9) 1.80(3)
B(5)-B(6) 1.83(3)
B(5)-H(5A) 1.1200
B(6)-B(11) 1.73(2)
B(6)-B(9) 1.77(3)
B(6)-H(6) 1.1200
B(7)-B(9) 1.76(3)
B(7)-B(11) 1.79(3)
B(7)-B(10) 1.76(3)
B(7)-B(12) 1.78(4)
B(7)-B(8) 1.82(3)
B(7)-H(7) 1.2400
B(8)-B(12) 1.78(3)
B(8)-B(11) 1.80(3)
B(8)-H(8) 1.1200
B(9)-B(11) 1.76(3)
B(9)-B(10) 1.78(3)
B(9)-H(9A) 1.1200
B(10)-B(12) 1.82(3)
B(10)-H(10A) 1.1200
B(11)-H(11) 1.1200
B(12)-H(12A) 1.2390

N(3)-Cu(1)-N(2) 174.7(5)
N(3)-Cu(1)-N(4)#1 91.3(4)
N(2)-Cu(1)-N(4)#1 88.5(4)
N(3)-Cu(1)-N(1)#2 90.4(4)
N(2)-Cu(1)-N(1)#2 89.9(4)
N(4)#1-Cu(1)-N(1)#2 177.5(5)
C(1)-N(1)-C(5) 117.8(12)
C(1)-N(1)-Cu(1)#3 122.3(10)
C(5)-N(1)-Cu(1)#3 119.5(9)
C(23)-N(4)-C(24) 119.5(12)
C(23)-N(4)-Cu(1)#4 122.1(9)
C(24)-N(4)-Cu(1)#4 118.0(9)

C(14)-N(3)-C(18)	116.9(12)
C(14)-N(3)-Cu(1)	122.1(9)
C(18)-N(3)-Cu(1)	120.9(9)
C(12)-N(2)-C(10)	118.1(11)
C(12)-N(2)-Cu(1)	120.2(9)
C(10)-N(2)-Cu(1)	121.3(9)
N(4)-C(23)-C(22)	124.0(13)
N(4)-C(23)-H(23)	118.0
C(22)-C(23)-H(23)	118.0
N(3)-C(18)-C(17)	123.8(14)
N(3)-C(18)-H(18)	118.1
C(17)-C(18)-H(18)	118.1
N(1)-C(5)-C(4)	121.6(14)
N(1)-C(5)-H(5)	119.2
C(4)-C(5)-H(5)	119.2
C(5)-C(4)-C(3)	118.7(15)
C(5)-C(4)-H(4)	120.6
C(3)-C(4)-H(4)	120.6
N(4)-C(24)-C(25)	121.8(14)
N(4)-C(24)-H(24)	119.1
C(25)-C(24)-H(24)	119.1
N(3)-C(14)-C(15)	124.2(14)
N(3)-C(14)-H(14)	117.9
C(15)-C(14)-H(14)	117.9
N(2)-C(10)-C(9)	120.4(13)
N(2)-C(10)-H(10)	119.8
C(9)-C(10)-H(10)	119.8
C(10)-C(9)-C(8)	121.7(14)
C(10)-C(9)-H(9)	119.2
C(8)-C(9)-H(9)	119.2
N(1)-C(1)-C(2)	123.5(15)
N(1)-C(1)-H(1)	118.2
C(2)-C(1)-H(1)	118.2
C(8)-C(13)-C(12)	121.0(15)
C(8)-C(13)-H(13)	119.5
C(12)-C(13)-H(13)	119.5

C(16)-C(17)-C(18)	118.6(15)
C(16)-C(17)-H(17)	120.7
C(18)-C(17)-H(17)	120.7
C(21)-C(22)-C(23)	118.4(14)
C(21)-C(22)-H(22)	120.8
C(23)-C(22)-H(22)	120.8
N(2)-C(12)-C(13)	121.9(14)
N(2)-C(12)-H(12)	119.1
C(13)-C(12)-H(12)	119.1
C(7)-C(6)-C(3)	178(2)
C(21)-C(25)-C(24)	118.4(13)
C(21)-C(25)-H(25)	120.8
C(24)-C(25)-H(25)	120.8
C(13)-C(8)-C(9)	116.5(13)
C(13)-C(8)-C(7)	122.3(15)
C(9)-C(8)-C(7)	121.1(15)
C(2)-C(3)-C(4)	118.4(14)
C(2)-C(3)-C(6)	122.1(15)
C(4)-C(3)-C(6)	119.5(15)
C(20)-C(19)-C(16)	176(2)
C(17)-C(16)-C(15)	119.8(14)
C(17)-C(16)-C(19)	123.5(16)
C(15)-C(16)-C(19)	116.6(15)
C(25)-C(21)-C(22)	117.8(12)
C(25)-C(21)-C(20)	116.1(14)
C(22)-C(21)-C(20)	126.0(15)
C(1)-C(2)-C(3)	119.4(15)
C(1)-C(2)-H(2)	120.3
C(3)-C(2)-H(2)	120.3
C(19)-C(20)-C(21)	178(2)

Table S4. Crystal data and structure refinement for BSF-21

Empirical formula	C20 H27 B12 Cu I N8
Formula weight	699.67
Temperature	1.360
Wavelength	0.71073 Å
Crystal system	orthorhombic
Space group	Pnna
Unit cell dimensions	a = 19.924(8) Å α= 90° b = 10.286(4) Å β= 90° c = 16.677(6) Å γ = 90°
Volume	3418(2) $Å^3$
Z	4
Density (calculated)	1.360 g/cm^3
Absorption coefficient	1.567 mm^{-1}
Goodness-of-fit on F^2	1.004
R indices [I>2sigma(I)]	R1 = 0.1575, wR2 = 0.2709
R indices (all data)	R1 = 0.0957, wR2 = 0.2270

Table S5 Selected bond lengths [Å] for BSF-21

Cu1 N1	2.005(7)
Cu1 N1	2.005(7)
Cu1 N4	2.021(7)
Cu1 N4	2.021(7)

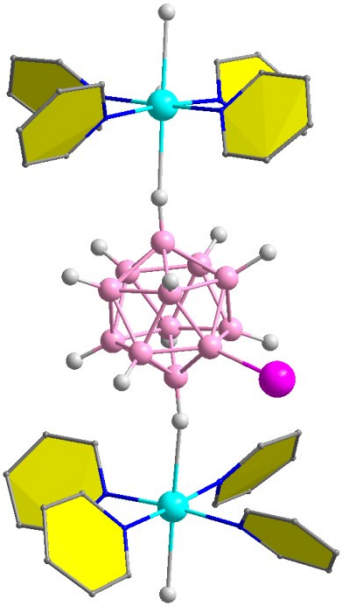

Fig. S1: Partial structures of BSF-2 and BSF-21 highlighting the $[B_{12}H_{11}I]^{2-}$ pillars,

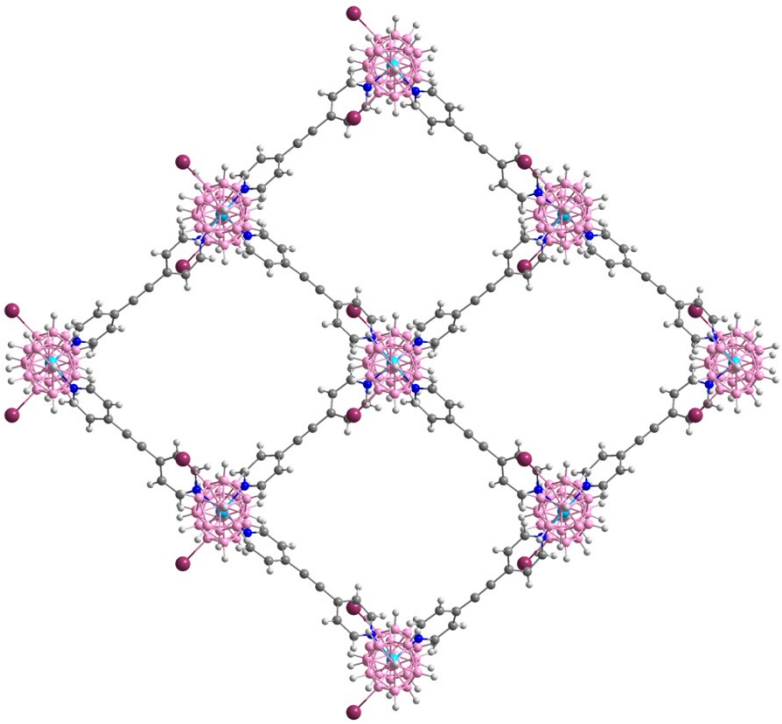

Fig. S2. 2D square layer of BSF-2

III Sorption Isotherms

Table S6. Langmuir-Freundlich parameters fit for C_3H_8, C_2H_6, CO_2, C_2H_2 and CH_4 in BSF-2 at 298 K.

	Site A			Site B			correlation coefficient (R)
	$q_{A,sat}$ (mol/kg)	b_A (kPa^{-1})	(R)	$q_{B,sat}$ (mol/kg)	b_B (kPa^{-1})	V_B	
C_3H_8	0.6068	2.261514	1.767981	4.48522	0.030769	0.521303	0.999854
C_2H_6	2.286567	0.0264	0.65113	0.409894	0.009136	2.221695	0.999945
CO_2	2.549627	0.009202	0.009202	0.267835	1.64E-13	7.757769	0.999997
C_2H_2	0.706287	0.04483	1.573618	6.402589	0.01586	0.567392	0.999956
CH_4	0.596877	0.006052	0.892831	0.109027	2.50E-06	2.942542	0.999925

Table S7. Langmuir-Freundlich parameters fit for C_3H_8, C_2H_6, CO_2, C_2H_2 and CH_4 in BSF-2 at 273 K.

	Site A			Site B			correlation coefficient (R)
	$q_{A,sat}$ (mol/kg)	b_A (kPa^{-1})	V_A	$q_{A,sat}$ (mol/kg)	b_A (kPa^{-1})	V_B	
C_3H_8	2.473521	0.0821769	0.568717	0.66467	7.41494	1.2509	0.999928
C_2H_6	1.807439	0.075599	0.712973	0.341872	0.162207	2.021514	0.999988
CO_2	3.304472	0.019365	0.895212	0.392958	3.74E-06	4.83235	0.999987
C_2H_2	3.366333	0.069638	0.605651	0.593441	0.460599	1.503002	0.999967
CH_4	0.00143	32424.86	4.776305	5.153295	0.001432	0.91344	0.999996

Table S8. Langmuir-Freundlich parameters fit for C_3H_8, C_2H_6, CO_2, C_2H_2 and CH_4 in BSF-2 at 313 K.

	Site A			Site B			correlation coefficient
	$q_{A,sat}$ (mol/kg)	b_A (kPa^{-1})	(R)	$Q_{B,sat}$ (mol/kg)	b_A (kPa^{-1})	V_B	(R)
C_3H_8	158.9548	0.0013	0.768608	0.838101	0.553853	1.353025	0.999934
C_2H_6	1.285557	0.028647	0.96738	0.117193	1.09E-9	7.342207	0.999981
CO_2	0.201085	9.89E-24	11.97349	2.956146	0.005411	0.945073	0.999991
C_2H_2	2.676052	0.035932	0.786344	0.099039	1.17E-11	9.061228	0.999977
CH_4	3.71429	3.71E-5	1.42361	0.187903	0.021855	0.753305	0.999935

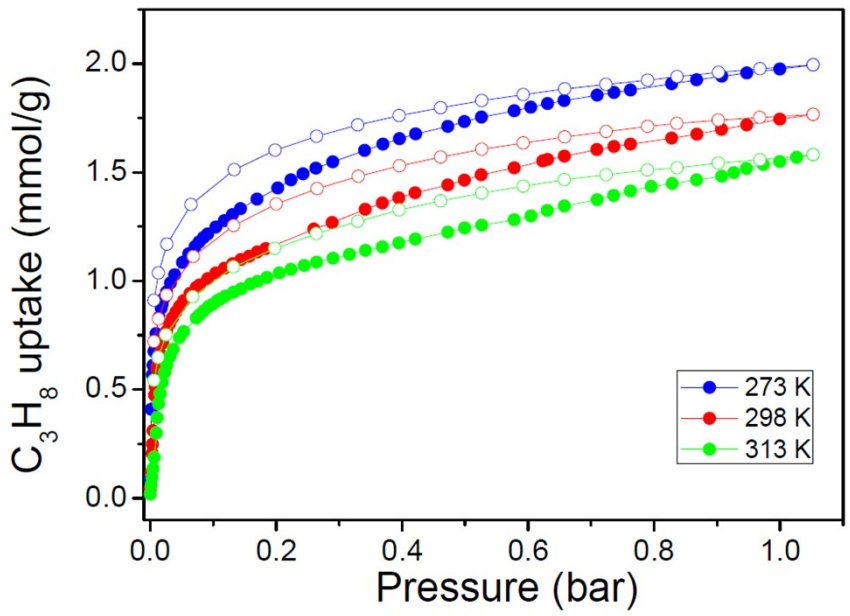

Fig. S3. Sorption isotherms of C_3H_8 on BSF-2 at temperature from 273 to 313 K

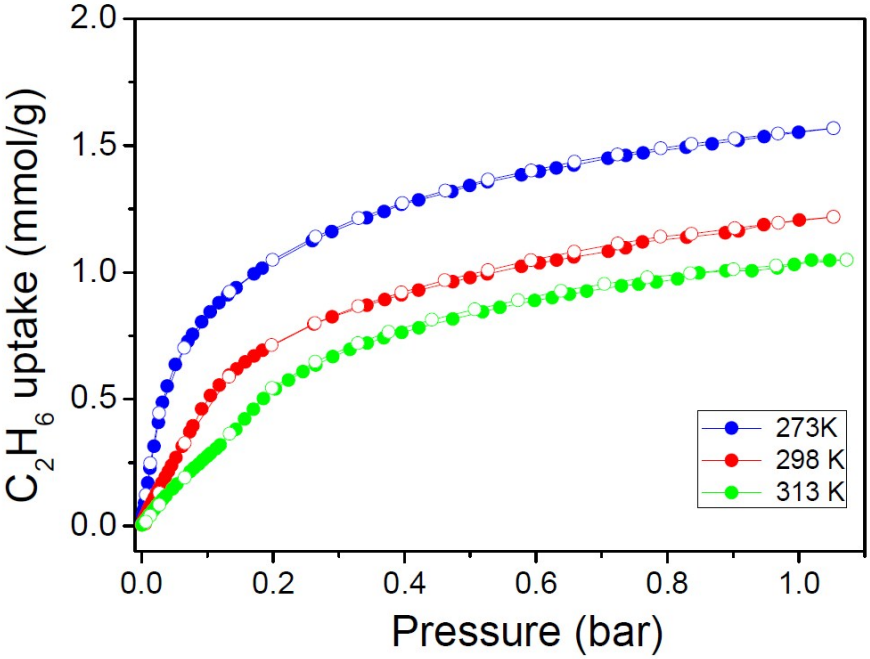

Fig. S4. Sorption isotherms of C_2H_6 on BSF-2 at temperature from 273 to 313 K.

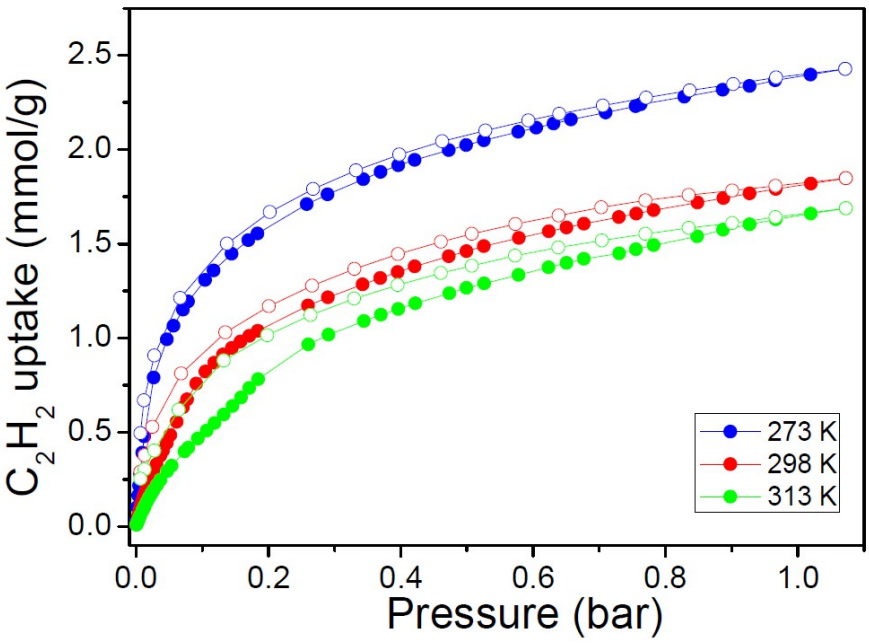

Fig. S5. Sorption isotherms of C_2H_2 on BSF-2 at temperature from 273 to 313 K

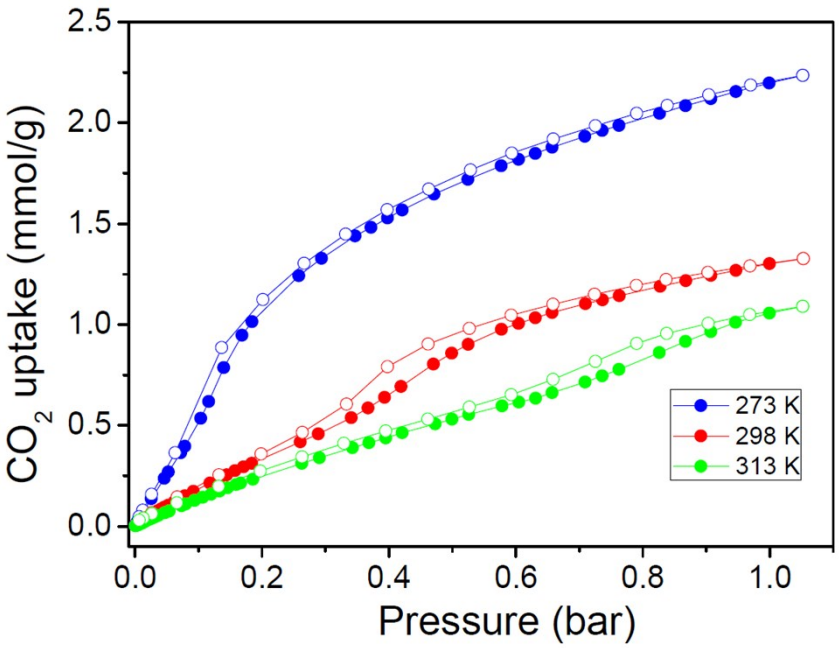

Fig. S6. Sorption isotherms of CO_2 on BSF-2 at temperature from 273 to 313 K.

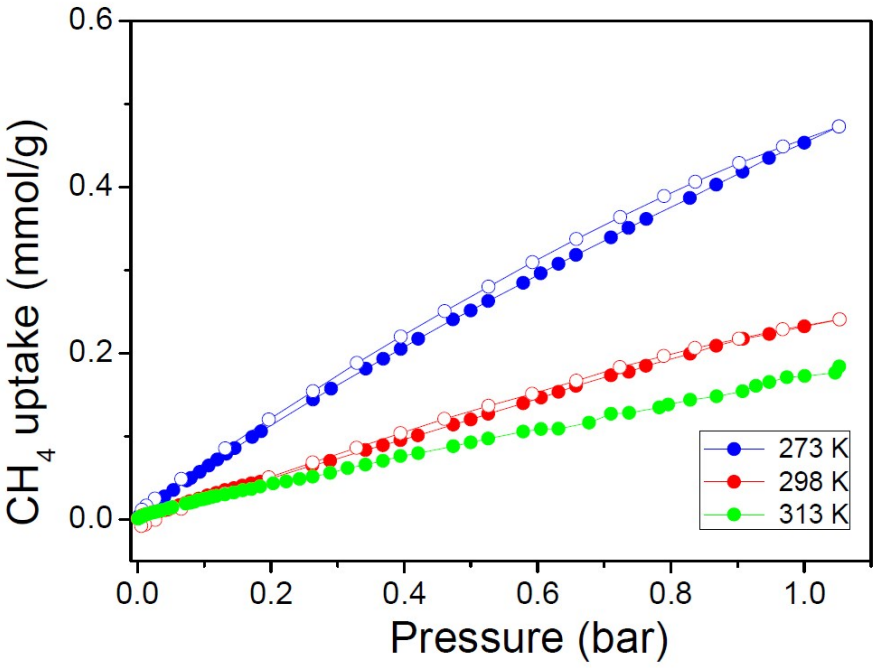

Fig. S7. Sorption isotherms of CH_4 on BSF-2 at temperature from 273 to 313 K.

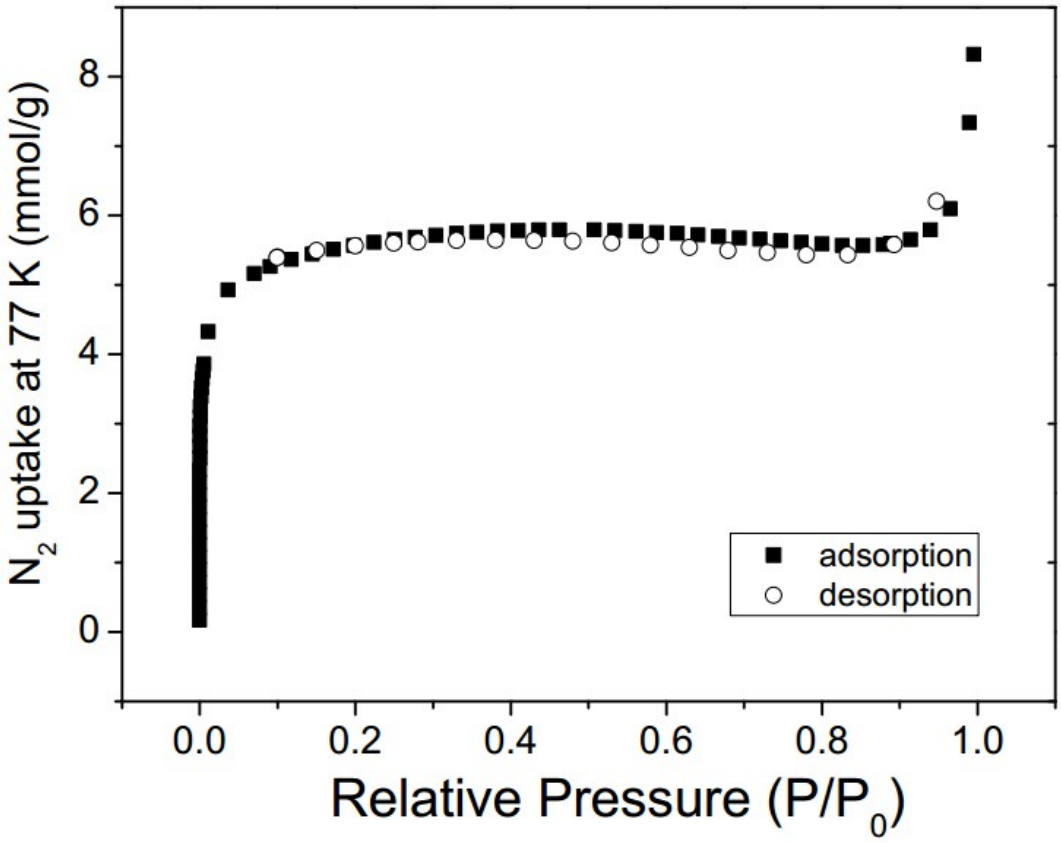

Fig. S8. The adsorption and desorption isotherm of N_2 on BSF-2 at 77 K. The calculated BET surface area and Langmuir surface area of BSF-2 by N_2 adsorption isotherm at 77 K is 403.3537 m^2/g and 556.8187 m^2/g.

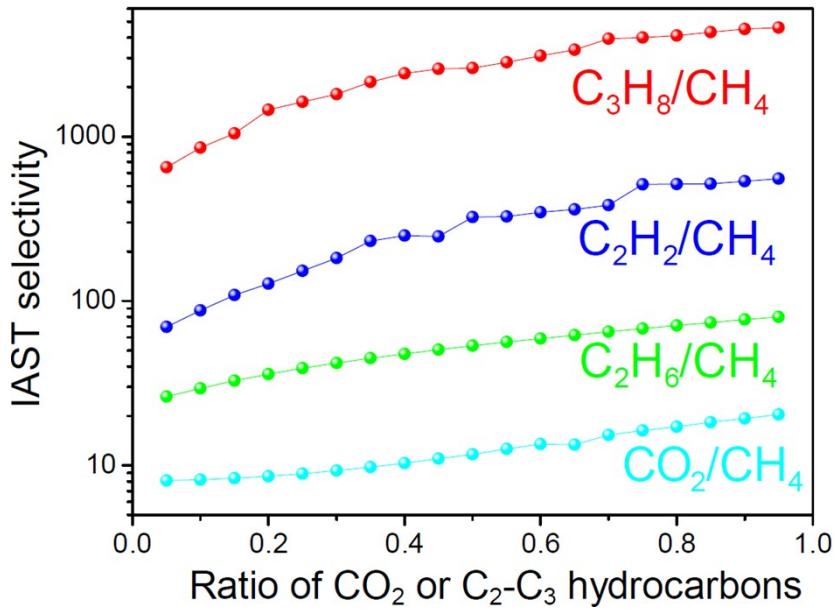

Fig. S9 IAST selectivity with different CO_2, C2 or C3 ratios in the gas mixture of C_3H_8/CH_4, C_2H_6/CH_4, C_2H_2/CH_4 and CO_2/CH_4.

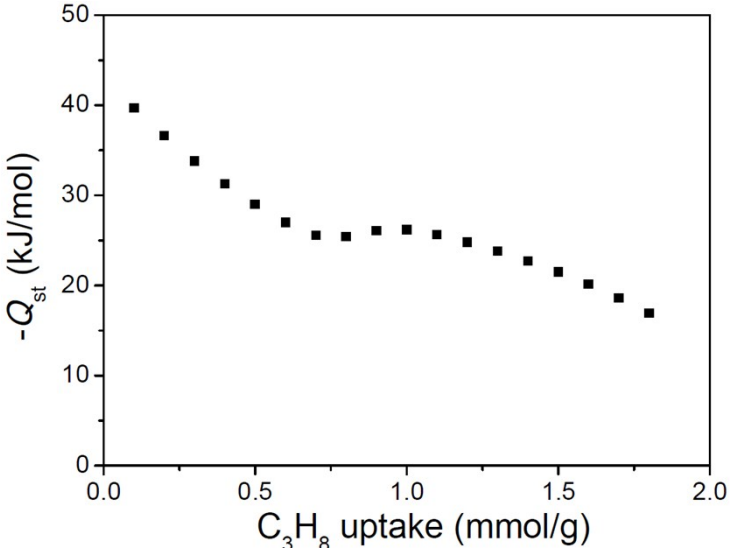

Fig. S10. Isosteric enthalpy of adsorption (Q_{st}) of BSF-2 towards C_3H_8.

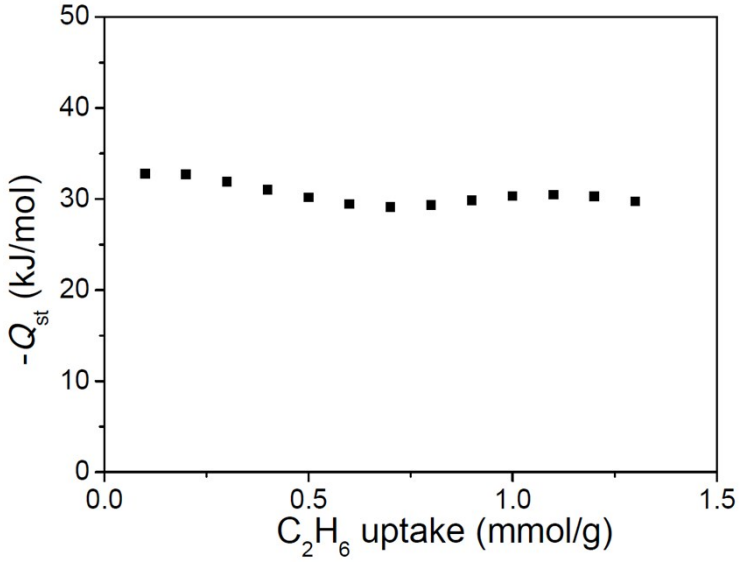

Fig. S11. Isosteric enthalpy of adsorption (Q_{st}) of BSF-2 towards C_2H_6.

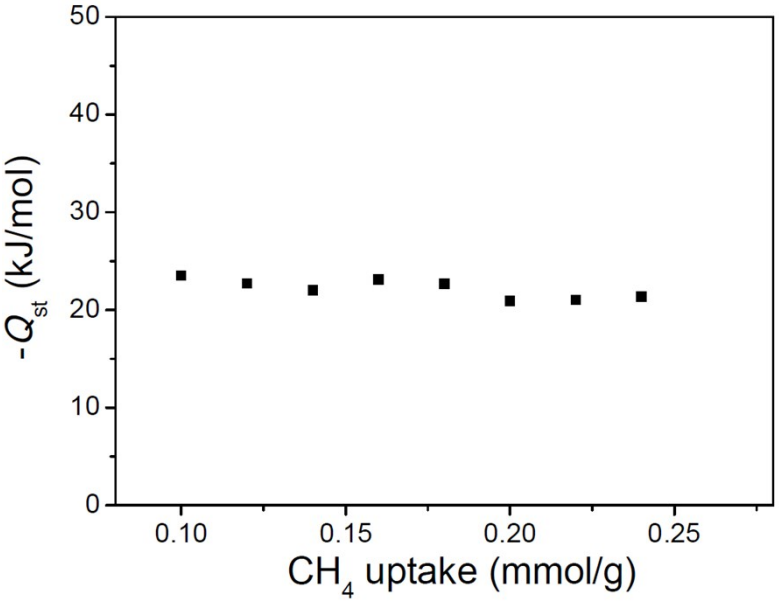

Fig. S12. Isosteric enthalpy of adsorption (Q_{st}) of BSF-2 towards CH_4.

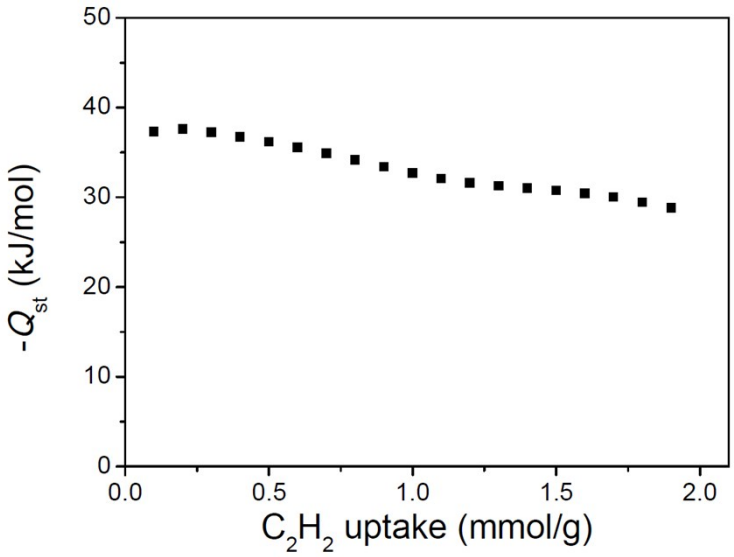

Fig. S13. Isosteric enthalpy of adsorption (Q_{st}) of BSF-2 towards C_2H_2.

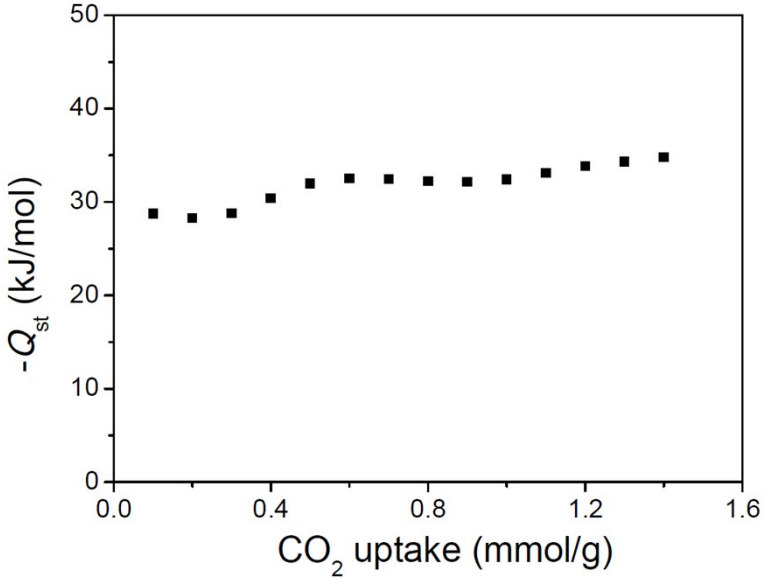

Fig. S14. Isosteric enthalpy of adsorption (Q_{st}) of BSF-2 towards CO_2.

Table S9 Summary of crystallographic parameters and gas adsorption data (297 K) of BSF-1 and BSF-2

	BSF-1	BSF-2
Composition	$\{CuB_{12}H_{12}(bpa)_2\}_n$	$\{CuB_{12}H_{11}I(bpa)_2\}_n$
Space group	C2/c	C2/c
a (Å)	28.764(2)	28.398(2)
b (Å)	17.1839(11)	17.7840(12)
c (Å)	19.918(3)	20.2046(15)
α	90	90
β	133.107(2)	133.929(2)
γ	90	90
ρ_{calc} (g/cm^3)	1.046	1.250
BET surface area (m^2/g)	535	403
Langmuir surface area (m^2/g)	830	557
Pore volume (cm^3/g)[a]	0.25 (0.27)	0.19 (0.20)
C_2H_2 uptake (cm^3/cm^3)	55.0	51.7
CO_2 uptake (cm^3/cm^3)	41.5	37.2
C_3H_8 uptake (cm^3/cm^3)	45.5	49.5
C_2H_6 uptake (cm^3/cm^3)	36.8	34.1
CH_4 uptake (cm^3/cm^3)	11.0	6.7
C_2H_2 Q_{st} (kJ/mol)	-30.7	-37.0
CO_2 Q_{st} (kJ/mol)	-21.7	-28.7
C_3H_8 Q_{st} (kJ/mol)	-33.7	-39.7
C_2H_6 Q_{st} (kJ/mol)	-28.1	-32.8
CH_4 Q_{st} (kJ/mol)	-23.7	-23.5

[a] values detected by 77 K N_2 adsorption (values calculated from single crystal data)

Table S10. Comparison of reported materials on IAST selectivity towards gas mixtures of C_3H_8/CH_4 and C_2H_6/CH_4

Material name (feature)	Pore sizes (Å or Å^2)	BET surface areas (m^2/g)	C_3H_8/CH_4 IAST selectivity[a]	C_2H_6/CH_4 IAST selectivity[a]	Ref
JUC-100	14	2040	80	11	Chem. Eur. J. 2014, 20, 9073
JUC-103	10	1484	55	8	Chem. Eur. J. 2014, 20, 9073
JUC-106	8	1122	75	13	Chem. Eur. J. 2014, 20, 9073
UTSA-35a	7.7 × 5.8	742.7	80	20	Chem. Commun., 2012, 48, 6493
UTSA-36a	3.1-4.4			16.6[b]	Chem. Eur. J. 2011, 17, 7817
MAF-49	3.3 × 3.0			170 (316K)	Nat. Commun 2015, 6, 8697
IRMOF-8		1360		8 (316K)	ACS Appl. Mater. Interfaces 2014, 6, 12093
Cu-TDPAH (OMS)		2171		16	J. Mater. Chem. A 2014, 2, 15823
SBMOF-2		145		25	Chem. Mater 2016, 28, 1636
Fe-MOF-74 (OMS)	11	1350	23[b]/(18)	5[b]	Science 2012, 335, 1606 (Inorg. Chem. 2016, 55, 3928)
PHA (carbon)		284		25	J. Mater. Chem. A 2016, 4, 2263
NAHA-1 (carbon)		895		32.6	J. Mater. Chem. A 2016, 4, 2263
NAHA-2 (carbon)		1192		23.9	J. Mater. Chem. A 2016, 4, 2263
NAHA-4 (carbon)		1538		18.4	J. Mater. Chem. A 2016, 4, 2263
Na-ETS-10 (zeolite)	8			45[e]	Chem. Eng. Sci 2011, 66, 1697
Ba/H-ETS-10	~8			15[e]	Chem. Eng. Sci 2011, 66, 1697

(zeolite)					
Ba-ETS-10 (zeolite)	~8			32[e]	Chem. Eng. Sci 2011, 66, 1697
Ext-MCM-41 (mesoporous)	15-200	470		12	Green Chem. 2011, 13, 1251
MCM-41 (mesoporous)	15-200	1090		6	Green Chem. 2011, 13, 1251
Ext-PCH (mesoporous)	15-200	470		10	Green Chem. 2011, 13, 1251
PCH (mesoporous)	15-200	814		5	Green Chem. 2011, 13, 1251
Zr-FUM	5/7	735	292		Ind. Eng. Chem. Res. 2017, 56, 14633
Zr-1,4-NDC	6/8	876	73.5		Ind. Eng. Chem. Res. 2017, 56, 14633
Zr-BDC	8/11	1200	71.5		Ind. Eng. Chem. Res. 2017, 56, 14633
Zr-2,6-NDC	11/14	1717	49.2		Ind. Eng. Chem. Res. 2017, 56, 14633
Zr-BPDC	12/16	2500	65.0		Ind. Eng. Chem. Res. 2017, 56, 14633
UiO-67	10.90/ 13.58	2590.63	73.7[c]	8.1[d]	Ind. Eng. Chem. Res. 2017, 56, 8689.
JXNU-4	9.8 × 9.8	1250	144[e] (273K)	14.6[e]	Inorg. Chem. 2017, 56, 2919
FIR-7a				14.6	Chem. Commun., 2013, 49, 11323
FIR-51	7.6 × 7.6	918.6	75	15	Dalton Trans. 2015, 44, 2893
Mg-MOF-74 **(OMS)**				11.5	Dalton Trans. 2015, 44, 2893
Co-MOF-74 **(OMS)**				7.5	Dalton Trans. 2015, 44, 2893
NOTT-101				12	Dalton Trans. 2015, 44, 2893
JLU-Liu5		707	107.8	17.6	Chem. Commun. 2014, 50, 8648.
JLU-Liu6		544	274.6	20.4	Chem. Commun. 2014, 50, 8648.
JLU-Liu18		1300	108.2	13.1	J. Mater. Chem.

					A.2015, 3,16627.
JLU-Liu22 (OMS)	10/13/18	1487	271.5	14.4	Chem. Commun. 2015, 51, 15287.
JLU-Liu34	12	2619	45.9	8.7	Cryst. Growth Des. 2017, 17, 2131.
JLU-Liu36	12	2497	40	8	Cryst. Growth Des. 2017, 17, 2131.
JLU-Liu37	8.6-11	1795	206	11	Inorg. Chem. 2017, 56, 4141
JLU-Liu38	8.6-11	1784	98	15	Inorg. Chem. 2017, 56, 4141.
FIR-7a-ht		1894.1	78.8[c]	14.6 [c]	Chem. Commun. 2013, 49, 11323.
FJI-C1 (anionc MOF)	7/11	1726.3	471	22	ChemSusChem 2014, 7, 2647.
FJI-C4 (anionc MOF)	5.9 × 5.9	690	293.4	39.7	ACS Appl. Mater. Interfaces 2016, 8, 9777
1-mim	10.2	940.26	200 (297K)	18 (297K)	Inorg. Chem. 2016, 55, 3928
1-eim	10.2	877.41	80 (297K)	12 (297K)	Inorg. Chem. 2016, 55, 3928
1-pim	10.2	839.04	75 (297K)	12 (297K)	Inorg. Chem. 2016, 55, 3928
1-buim	10.2	769.67	50 (297K)	11 (297K)	Inorg. Chem. 2016, 55, 3928
MFM-202a (Flexible)	9 × 9	2220	87	10	Chem. Mater. 2016, 28, 2331
tbo-MOF-1 (HKUST-1-like)	17.8 × 18.3		32[e]	5[e]	RSC Adv. 2014, 4, 63855
tbo-MOF-2 (HKUST-1-like)	17.8 × 18.3		60[e]	14[e]	RSC Adv. 2014, 4, 63855
Zn_6 $(2\text{-mbim})_2$	14	630	90 (285K)	20 (285K)	Cryst. Growth Des. 2014, 14, 6467
InOF-1	7.4	1108.6	90	17	Ind. Eng. Chem. Res. 2017, 56, 4488
LIFM	12.1	803	35.8 [d]	9[d]	Cryst. Growth Des. 2017, 17, 1476
BSF-1		535	353	23	Angew. Chem. Int

					Ed. 2019, 58, 8145
BSF-2		**403**	**2609**	**53**	**This work**

[a] calculated using the ideal adsorption solution theory under the condition of equimolar binary mixtures and 1 bar;
[b] gas adsorption selectivity data obtained from Henry's law;
[c] IAST selectivity calculated using the ideal adsorption solution theory under the condition of C2/C1 or C3/C1 = 5/85 and 1 bar.
[d] IAST selectivity calculated using the ideal adsorption solution theory under the condition of 1 bar (unspecified molar ratio).
[e] Calculated using the ideal adsorption solution theory under the condition of C2/C1 or C3/C1 = 0.05/0.95 and 1 bar.
Note: OMS = open metal sites.

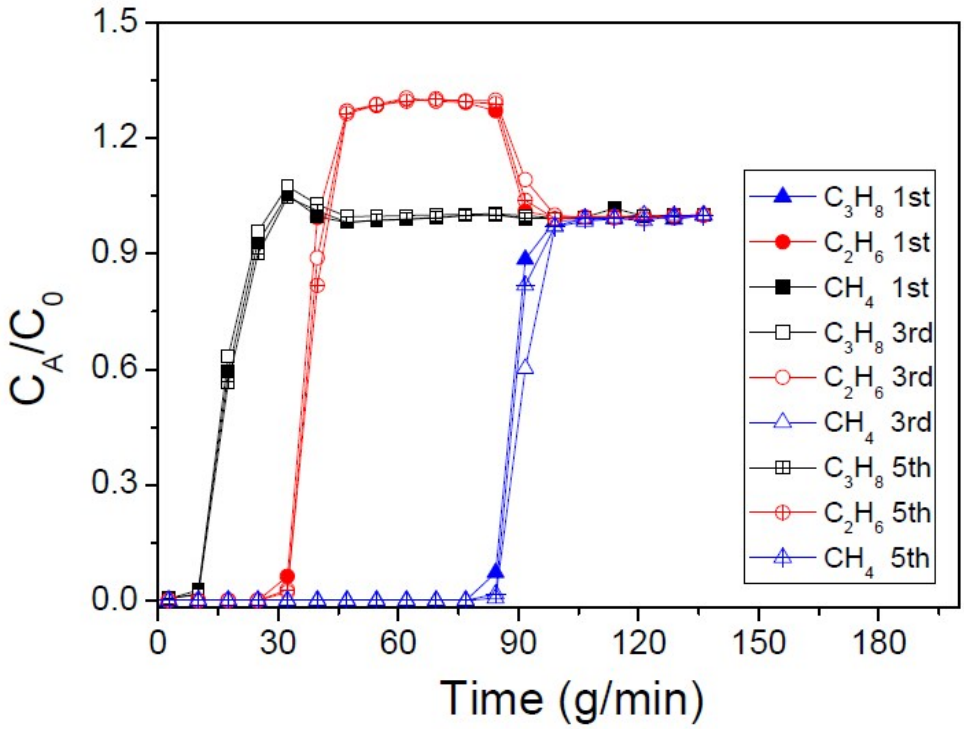

Fig. S15. Stacked Column breakthrough experiments (Φ 0.46 cm × 5 cm) of $C_3H_8/C_2H_6/CH_4$ (5/10/85) on BSF-2 at 4.0 mL/min.

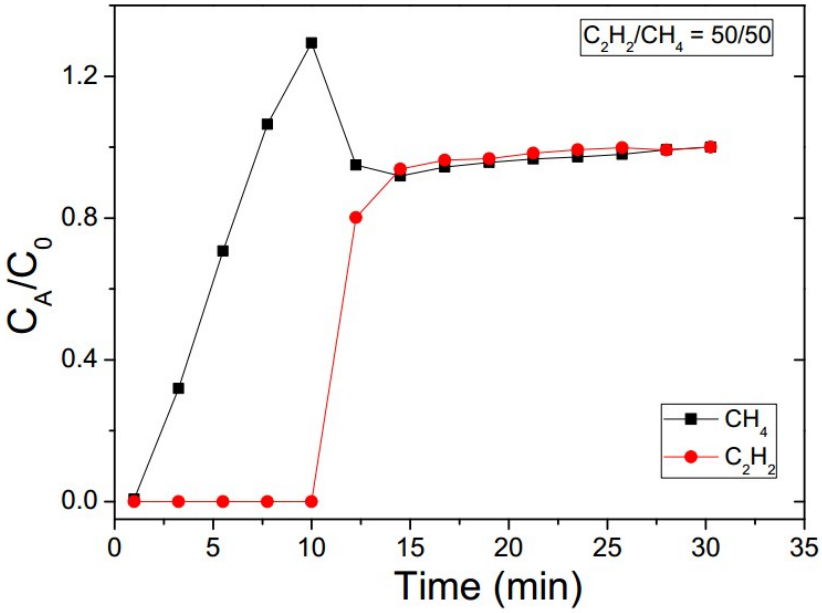

Fig. S16. Stacked Column breakthrough experiments (*Φ* 0.46 cm × 5 cm) of C_2H_2/CH_4 (50/50) on BSF-2 (0.2808 g) at 3.5 mL/min.

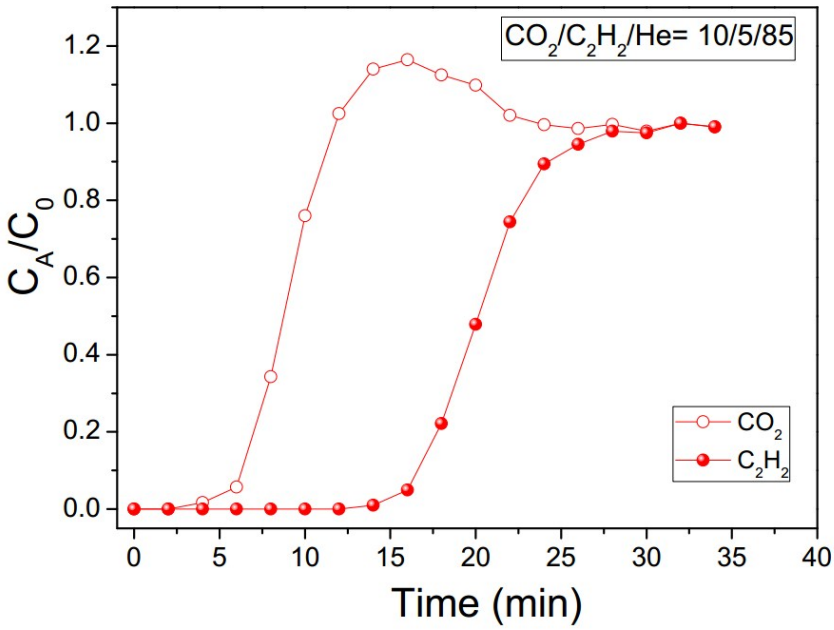

Fig. S17. Stacked Column breakthrough experiments (*Φ* 0.46 cm × 5 cm) of $C_2H_2/CO_2/He$ (5/10/85) on BSF-2 (0.2808 g) at 3.3 mL/min. This gas mixture compositions simulate the practical relative proportions of C_2H_2 and CO_2 in gas streams for acetylene production. The role of He is to serve as an inert carrier gas.

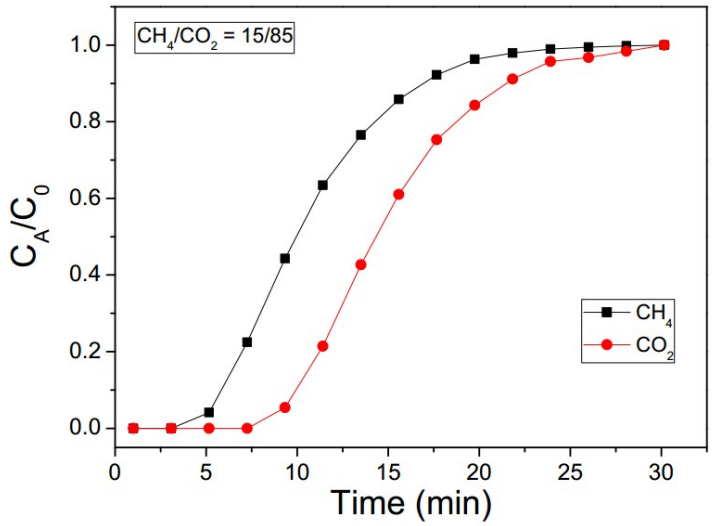

Fig. S18. Stacked Column breakthrough experiments (Φ 0.46 cm × 5 cm) of CO_2/CH_4 (15/85) on BSF-2 (0.2808 g) at 3.0 mL/min. This gas mixture compositions simulate the practical relative proportions of CO_2 and CH_4 in natural gas.

Table S11 Comparision of the experimental Q_{st} (in kJ/mol) on BSF-2 and BSF-1 calculated using the Clausius-Clapeyron equation

Gas molecules	Low coverage experimental Q_{st} (kJ/mol)		ΔQ_{st} = Q_{st} *(BSF-2)*- Q_{st} *(BSF-1)* (kJ/mol)
	BSF-2	BSF-1	
C_3H_8	-39.7	-33.7	-6.0
C_2H_6	-32.8	-28.6	-4.2
CH_4	-23.5	-23.7	+0.2
C_2H_2	-37.3	-30.7	-6.6
CO_2	-29.3	-21.7	-7.6

IV PXRD, TGA and IR Data

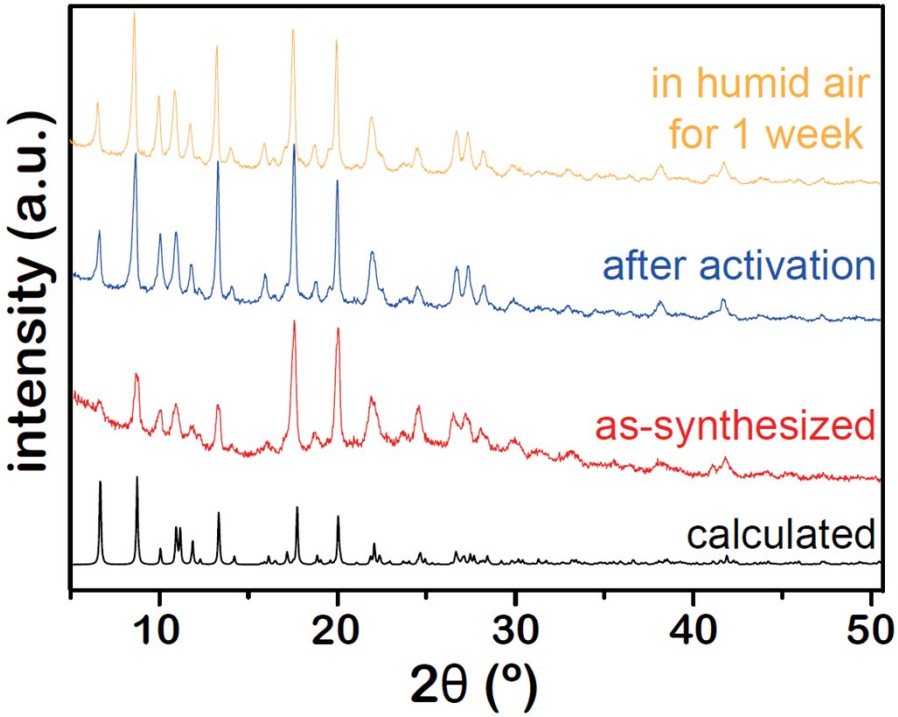

Fig. S19. Powder X-ray diffraction (XRD) patterns calculated from crystal X-ray structure data (black) of BSF-2, as-synthesized BSF-2 (red)，activated BSF-2 (blue)，activated BSF-2 exposed to humid air (~75% humidity) for a week (brown).

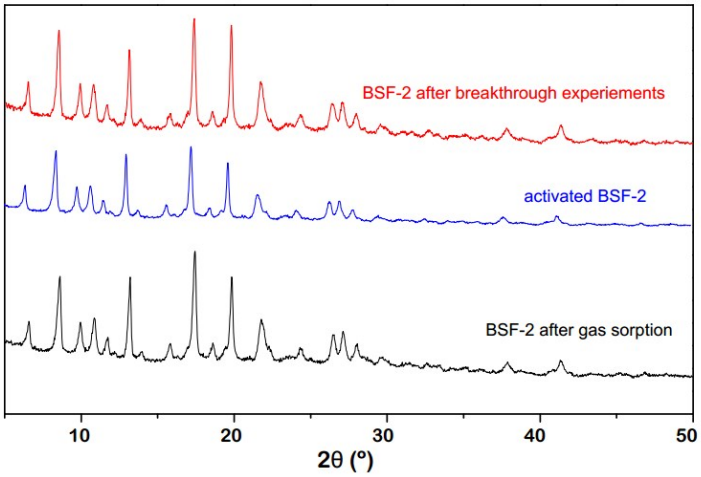

Fig. S20. Powder X-ray diffraction (XRD) patterns from activated BSF-2 (blue)，BSF-2 after gas sorption (black) and BSF-2 after breakthrough experiments (red).

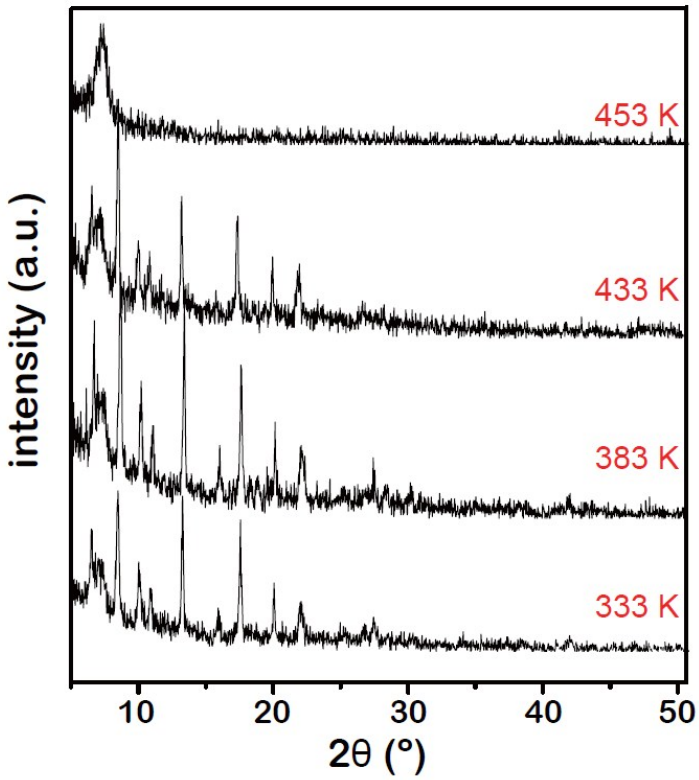

Fig. S21. Temperature varied powder X-ray diffraction (XRD) patterns. It indicates the decomposition temperature was ~433 K (160 ºC).

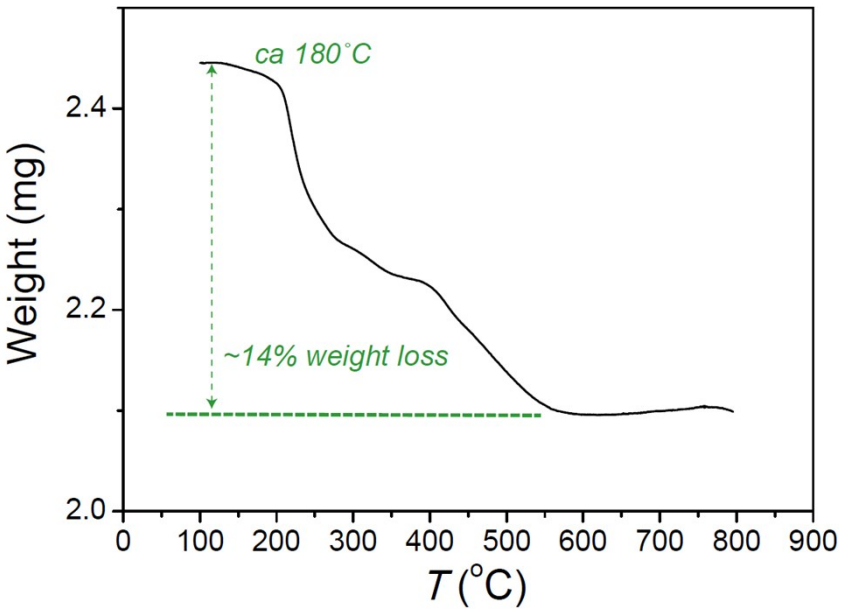

Fig. S22. TGA curves of BSF-2

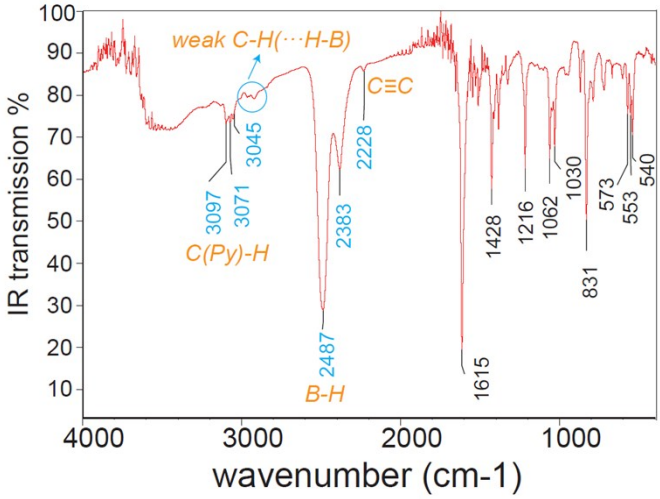

Fig. S23. IR spectrum of BSF-2

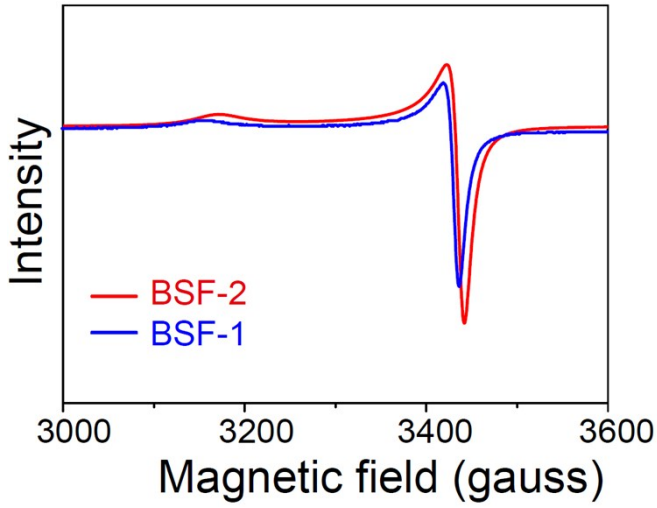

Figure S24. EPR spectra of BSF-2 and BSF-1.

Analysis: the positions of $g_{\perp}$ (in the right) and $g_{/\!/}$ (in the left) signals implied the unpaired electron was localized in the d_{z2} orbital of Cu(II), confirming an octahedral coordiation field with an axial elongation distortion. The $g_{\perp}$ values are both 2.054 for BSF-2 and BSF-1, consistent with the structures that both materials have four bpa ligands coordinating to the Cu(II) centers in the equatorial positions. The $g_{/\!/}$ value are 2.225 and 2.232 for BSF-2 and BSF-1, respectively, indicating that $[B_{12}H_{11}I]^{2-}$ is less coordinating to Cu(II) in the axial positions than $[B_{12}H_{12}]^{2-}$, which can be explained by the substitution of I-group leading to higher steric hindance and replusion bewteen dodecaborates and the sql network. The corresponding calculated G values are 4.16 and

4.30, suggesting a negligible exchange interaction between Cu(II)-Cu(II) as the distances are more than 10 Å.

V. DFT Calculation

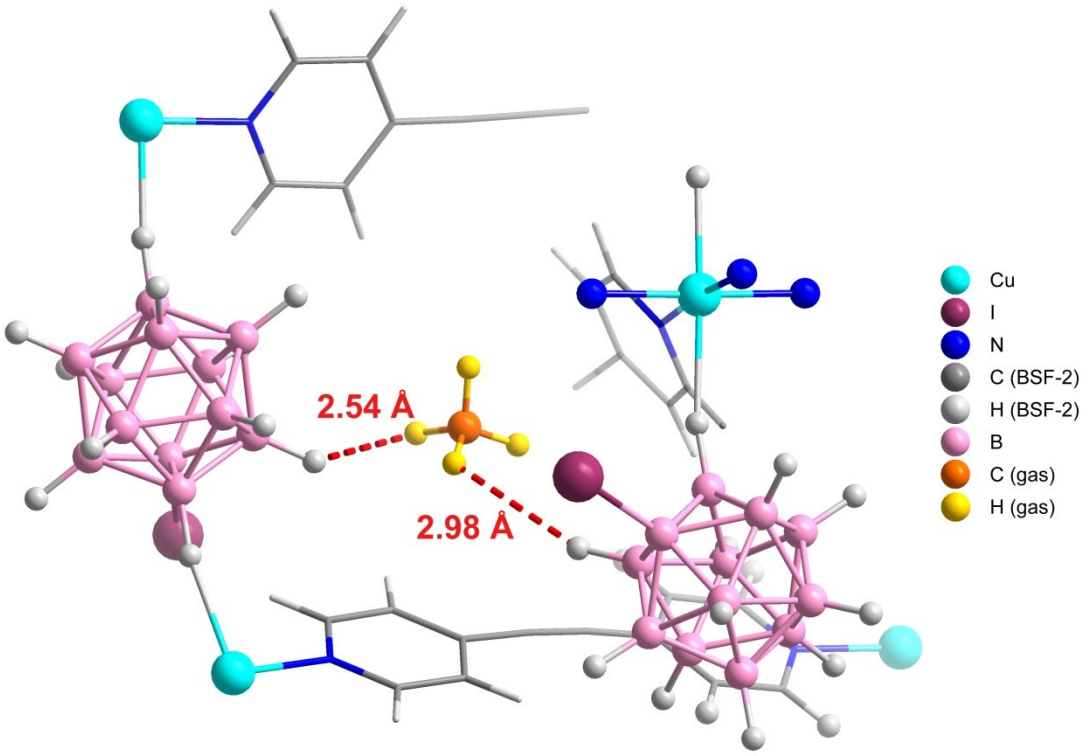

Fig. S25. Optimized CH_4 adsorption configuration in BSF-2.

Table S12 Comparison of DFT calculated potential energies (in kJ/mol) for single C_3H_8, C_2H_6, CH_4, C_2H_2 and CO_2 molecules located in the optimal BSF-2 and BSF-1

Gas molecules	DFT calculated sorbate-sorbent energy *E* (k*J/mol)*		*ΔE=E(BSF-2)- E(BSF-1)* (kJ/mol)
	BSF-2	BSF-1	
C_3H_8	58.3999	47.048	11.3519
C_2H_2	42.9561	35.7082	7.2479
CH_4	26.1486	25.4521	0.6965

References

[1] W. H. Knoth, H. C. Miller, J. C. Sauer, J. H. Balthis, Y. T. Chia and E. L. Muetterties, *Inorg Chem.* **1964**, *3*, 159–167.

[2] X. Cui, K. Chen, H. Xing, Q. Yang, R. Krishna, Z. Bao, H. Wu, W. Zhou, X. Dong, Y. Han, B. Li, Q. Ren, M. J. Zaworotko, B. Chen, *Science.* **2016**, *353*, 141– 144.

[3] Y. Chen, Z. Qiao, D. Lv, H. Wu, R. Shi, Q. Xia, H. Wang, J. Zhou, Z. Li, *Ind. Eng. Chem. Res.* **2017**, 56, 4488–4495.